

High Fidelity Face Manipulation with Extreme Pose and Expression

Chaoyou Fu¹²³ Yibo Hu¹ Xiang Wu¹ Guoli Wang³ Qian Zhang³ Ran He^{12*}

¹ CRIPAC & NLPR, Institute of Automation, Chinese Academy of Sciences

² University of Chinese Academy of Sciences

³ Horizon Robotics

{chaoyou.fu, rhe}@nlpr.ia.ac.cn, yibo.hu@cripac.ia.ac.cn
alfredxiangwu@gmail.com, {guoli.wang, qian01.zhang}@horizon.ai

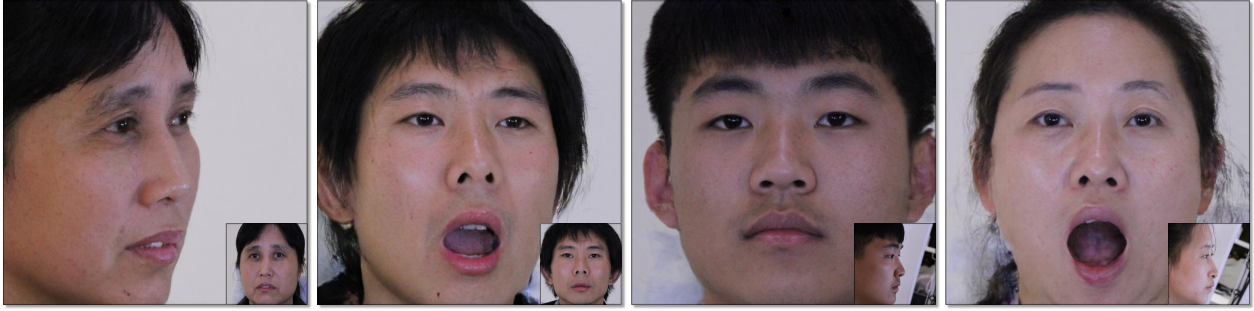


Figure 1: Synthesis results (512×512) on our MVF-HQ database. The lower right corner is the input face.

Abstract

Face manipulation has shown remarkable advances with the flourish of Generative Adversarial Networks. However, due to the difficulties of controlling the structure and texture in high-resolution, it is challenging to simultaneously model pose and expression during manipulation. In this paper, we propose a novel framework that simplifies face manipulation with extreme pose and expression into two correlated stages: a boundary prediction stage and a disentangled face synthesis stage. In the first stage, we propose to use a boundary image for joint pose and expression modeling. An encoder-decoder network is employed to predict the boundary image of the target face in a semi-supervised way. Pose and expression estimators are used to improve the prediction accuracy. In the second stage, the predicted boundary image and the original face are encoded into the structure and texture latent space by two encoder networks respectively. A proxy network and a feature threshold loss are further imposed as constraints to disentangle the latent space. In addition, we build up a new high quality Multi-View Face (MVF-HQ) database that contains 120K high-resolution face images of 479 identities with pose and expression variations, which will be released soon. Qualitative and quantitative experiments on four databases show that our method pushes forward the advance of extreme face

manipulation from 128×128 resolution to 1024×1024 resolution, and significantly improves the face recognition performance under large poses.

1. Introduction

Photo-realistic face manipulation with arbitrary pose and expression is a meaningful task in a wide range of fields, such as movie industry, entertainment and photography technologies. With the flourish of Generative Adversarial Networks (GANs) [9], face manipulation has achieved significant advances in recent years [7, 25, 16, 14, 27]. However, existing face manipulation methods mainly focus on only one facial variation (e.g., pose or expression). The methods for large pose or expression have still been limited to a low-resolution (128×128). Particularly, joint pose and expression modeling is challenging [40], especially when high-resolution facial images have extreme pose and expression.

For face manipulation, a straightforward way is to apply image-to-image translation [17, 33]. However, in the case of high-resolution with extreme pose and expression, it is difficult to guarantee the facial local structures in this way. As shown in Fig. 2 (a), the facial local structures, such as the eyes, nose and mouth, are unclear. Recent obser-

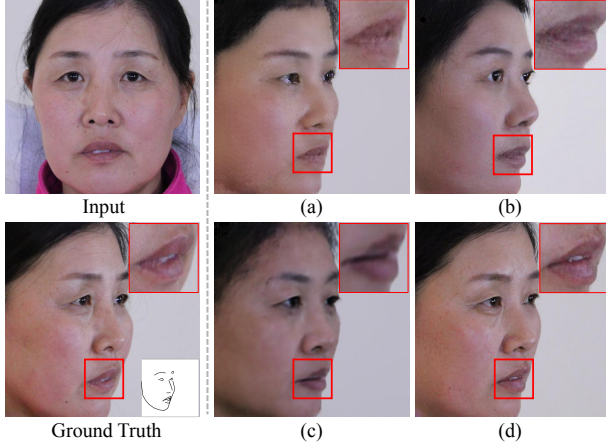


Figure 2: Visual comparisons (512×512) of different methods. (a) Direct image-to-image translation [33]. The local structures, e.g., the mouth, are unclear; (b) Directly concatenating the original input face and the boundary of the target face [14]. The local structures are ambiguous and textures are confused; (c) Directly utilizing a face recognition network to disentangle structure and texture [2]. The local structures are clear, but the textures are somewhat lost; (d) Our method. The structures and textures are well maintained.

variations in [33] show that the boundary information is crucial in high fidelity image synthesis. Hence, we argue that the lack of geometry guidance makes it difficult to synthesize extreme high-resolution face images. Several geometry guided methods have been proposed for face manipulation [14, 18, 29]. For example, CAPG-GAN [14] utilizes facial landmarks to control face rotation. SC-FEGAN [18] realizes local facial editing by sketch. Most of geometry guided methods directly concatenate a face image and its geometry guidance in the image space. However, since there is no disentanglement between the structure and texture, such the concatenation is difficult to maintain the facial structure and texture. As shown in Fig. 2 (b), the synthesized face’s structures are ambiguous and its textures are confused. [2] proposes a simple disentanglement manner. It introduces a face recognition network to learn structure invariant features, and then concatenates the structure invariant features with structure features to synthesize faces. As shown in Fig. 2 (c), this disentanglement manner does make the structure of the synthesized face clearer, but the textures of the synthesized high-resolution face are somewhat lost. We argue that it is because the features of the face recognition network are too compact, leading to severe texture loss in such high-resolution case.

Based on the above observations, we propose a novel framework for high-resolution face manipulation with extreme pose and expression, as shown in Fig. 3. Our frame-

work simplifies this challenging task into two correlated stages: a boundary prediction stage and a disentangled face synthesis stage. The first stage utilizes a boundary image for joint pose and expression modeling. It employs an encoder-decoder network to predict the boundary image of a target face in a semi-supervised way [26]. Pose and expression estimators are introduced to improve the prediction accuracy. The second stage encodes the predicted boundary image and the original face into the structure and texture latent space by two encoder networks respectively. A proxy network and a feature threshold loss are proposed to disentangle the latent space. Specifically, since it is hard to directly disentangle the structure and texture [28], we introduce a face recognition network as a proxy to facilitate disentanglement. Different from [2] that directly utilizes the compacted features of the proxy network, we propose a simple yet effective feature threshold loss to control the compactness between our learned face features and the compacted features, as shown in Fig. 3. Our method disentangles the structure and texture, while keeps the integrity of the texture, as shown in Fig. 2 (d). More high-resolution extreme face manipulation results are presented in Fig. 1 (512×512) and Fig. 5 (1024×1024).

Moreover, we introduce a new high quality Multi-View Face (MVF-HQ) database. It contains 120K high-resolution face images from 479 identities with diverse pose and expression variations, whose facial areas reach 2048×2048 resolution. We will release this database soon, along with its 5 precise facial landmarks annotated by human.

In summary, the main contributions are as follows:

- The high-resolution face manipulation problem with extreme pose and expression is formulated as a stage-wise learning problem that contains two correlated stages: a boundary prediction stage and a disentangled face synthesis stage.
- We realize joint pose and expression modeling by the boundary image translation in the first stage. Besides, a proxy network and a feature threshold loss are introduced in the second stage to disentangle the structure and texture for better utilizing the boundary image.
- This is the first time to explore extreme high-resolution face manipulation. A new high-resolution (2048×2048) face database is created. These works are expected to promote the development of high-resolution image synthesis.
- Experiments on the MultiPIE [10], RaFD [22], CelebA-HQ [19] and our MVF-HQ databases show that our method pushes forward the advance of extreme face manipulation from 128×128 resolution to 1024×1024 resolution, and significantly improves the face recognition performance under large poses.

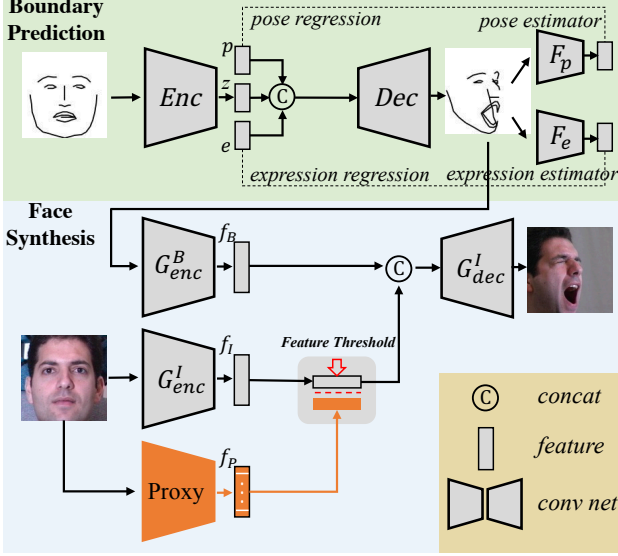


Figure 3: The framework of our method, which consists of a boundary prediction stage and a disentangled face synthesis stage. The first stage predicts the boundary image of the target face in a semi-supervised way. A pose estimator and an expression estimator is used to improve the prediction accuracy. The second stage utilizes the predicted boundary image to synthesize refined face. A proxy network and a feature threshold loss are introduced to disentangle the structure and texture in the latent space.

2. Related Work

2.1. Face Manipulation

Face manipulation has attracted great attention to computer vision and graphics [3, 34, 37, 6, 21, 30, 23]. Recently, Generative Adversarial Networks (GANs) [9] have shown great potential in the field of face manipulation. For example, StarGAN [7] realizes multi-domain face attribute transfer by a single generator. By controlling the magnitude of Action Units (AU), GANimation [25] renders expressions in a continuum. TP-GAN [16] realizes photo-realistic facial frontalization from a single image. FaceID-GAN [27] introduces an identity classifier as a competitor to better preserve identity when pose and expression change. However, extreme face manipulation methods [16, 27, 14] are still limited to low-resolution (128×128). High-resolution face manipulation with extreme pose and expression remains unexplored.

2.2. High Fidelity Image Synthesis

High fidelity image synthesis is a hot topic in computer vision community. It contains unconditional manner and conditional manner. Unconditional high-resolution image synthesis generates images from noise without any condi-

tion. PG-GAN [19] synthesizes high-resolution face images by progressively growing the generator and discriminator. It also introduces a 1024×1024 resolution CelebA-HQ database. IntroVAE [15] first utilizes variational model to synthesize high-resolution images without discriminator. For conditional high-resolution image synthesis, the synthesized images need to meet the given conditions. pix2pixHD [33] proposes a coarse-to-fine generator and a multi-scale discriminator for high fidelity image translation. Video-to-video [32] extends pix2pixHD with a spatio-temporal adversarial objective, achieving temporally coherent high-resolution video translation. BigGAN [4] first achieves high-resolution (512×512) conditional image synthesis on the Imagenet. StyleGAN [20] introduces an alternative generator to automatically learn attributes and releases a 1024×1024 resolution FFHQ database.

3. Method

Given an original face I^a , the goal of our method is to synthesize the target face I^b , according to a given pose vector p^b and an expression vector e^b . In addition, we denote the boundary image of the original face and the target face as B^a and B^b , respectively. In order to better realize high fidelity face synthesis with extreme pose and expression, we explicitly divide the face manipulation task into two stages: a boundary prediction stage and a disentangled face synthesis stage, as shown in Fig. 3. In the rest of this section, we will present the above two stages in detail.

3.1. Boundary Prediction

Boundary prediction stage predicts the target boundary image according to the given conditional vectors, including a pose vector and an expression vector. As shown in Fig. 3, we utilize an encoder network Enc and a decoder network Dec to realize this conditional boundary prediction. Specifically, through Enc , we first map the original input boundary image B^a into a latent space $z^a = Enc(B^a)$. Then, the pose vector p^b and expression vector e^b are concatenated with the hidden variable z^a to provide conditional information. Last, the target boundary image is generated by the decoder network $\hat{B}^b = Dec(z^a, p^b, e^b)$.

The pose and expression are discrete in the database, e.g., the MultiPIE database [10] only has 15 discrete poses and 6 discrete expressions. However, we expect that this stage can generate boundary image with arbitrary pose and expression, including the pose and expression existing in the database or beyond the database. Hence, we introduce a semi-supervised training manner. For the pose and expression in the database, we can utilize the corresponding ground truth to constrain the generated boundary image. For the pose and expression that do not exist in the database, we utilize two pre-trained estimators, including a pose estimator F_p and an expression estimator F_e , to constrain the

generated boundary image by conditional regression.

The loss functions involved in this stage are described below, including a pixel-wise loss and a conditional regression loss.

Pixel-Wise Loss. For the pose and expression that belong to the database, a pixel-wise L_1 loss is utilized to constrain the predicted boundary image $\hat{B}^b = Dec(Enc(B^a), p^b, e^b)$:

$$\mathcal{L}_{\text{pix-boud}} = |Dec(Enc(B^a), p^b, e^b) - B^b|, \quad (1)$$

where B^b is the ground truth target boundary image.

Conditional Regression Loss. For the pose and the expression that do not exist in the database, we first randomly produce p^r and e^r to generate boundary image $B^r = Dec(z^a, p^r, e^r)$. Then, we utilize a pose estimator F_p and an expression estimator F_e to estimate pose $\hat{p}^r = F_p(B^r)$ and expression $\hat{e}^r = F_e(B^r)$, respectively. The estimated \hat{p}^r and \hat{e}^r are used to constrain the generated boundary image. The intuition is that the estimated \hat{p}^r and \hat{e}^r of B^r should be equal to the conditional vectors p^r and e^r , respectively. Hence, a conditional regression loss, including a pose regression term and an expression regression term, is formulated as:

$$\mathcal{L}_{\text{reg}} = \|F_p(Dec(z^a, p^r, e^r)) - p^r\|_2^2 + \|F_e(Dec(z^a, p^r, e^r)) - e^r\|_2^2. \quad (2)$$

The parameters of the pre-trained F_p and F_e are fixed during training procedure.

3.2. Disentangled Face Synthesis

This stage utilizes the predicted boundary image to perform refined face synthesis. As shown in Fig. 3, we first utilize two encoders G_{enc}^B and G_{enc}^I to map the predicted boundary image \hat{B}^b and the original input face I^a to $f_{B^b} = G_{enc}^B(\hat{B}^b)$ and $f_{I^a} = G_{enc}^I(I^a)$, respectively. Then, we disentangle the structure and texture in the latent space, by a proxy network *Proxy* and a feature threshold loss. After disentanglement, the boundary features f_{B^b} and the image feature f_{I^a} are concatenated to feed into the decoder G_{dec}^I , synthesizing the final target face $\hat{I}^b = G_{dec}^I(f_{B^b}, f_{I^a})$.

The loss functions in this stage are presented below, including a feature threshold loss, a multi-scale pixel-wise loss, a multi-scale conditional adversarial loss and an identity preserving loss.

Feature Threshold Loss. The feature threshold loss is designed to assist in disentangling the structure and texture in the latent space. Considering that directly disentangling structure and texture is difficult, we utilize a pre-trained face recognition network as a proxy network *Proxy*, whose features $f_{Pa} = Proxy(I^a)$ are thought to be structure invariant. In addition, instead of directly utilizing the compact features f_{Pa} that will result in texture loss, as shown in

Fig. 2 (c), we introduce a feature threshold loss to better disentangle the structure and texture. Specifically, it controls the feature distance between the face features $f_{I^a} = G_{enc}^I(I^a)$ and the compact features $f_{Pa} = Proxy(I^a)$:

$$\mathcal{L}_{\text{thr}} = [\|G_{enc}^I(I^a) - Proxy(I^a)\|_2^2 - m]^+, \quad (3)$$

where $[\cdot]^+ = \max(0, \cdot)$ and m is a threshold value. As the loss \mathcal{L}_{thr} decreases, the face features f_{I^a} are closer to the compact features f_{Pa} , which means the structure and the texture are more disentangled. Meanwhile, the threshold value m controls the compact degree of face features f_{I^a} , which is used to maintain the texture. The parameter analysis of m is presented in Section 4.4.

Multi-Scale Pixel-Wise Loss. We introduce a multi-scale pixel-wise loss to constrain the synthesized face at different scales. Specifically, with the downsampling operation on factors of 2 and 4, we first obtain an image pyramid of 3 scales of the synthesized and the ground truth faces, respectively. Then, we calculate the pixel-wise loss on these 3 scales faces:

$$\mathcal{L}_{\text{pix-mul}} = \sum_{s=1,2,3} |G_{dec}^I(f_{B^b}, f_{I^a})_s - I_s^b|, \quad (4)$$

where s denotes the scales. The pixel-wise loss at the top of the image pyramid pays more attention to the global information, because it has a larger receptive field. On the contrary, the pixel-wise loss in the bottom of the image pyramid is more concerned with the recovery of details.

Multi-Scale Conditional Adversarial Loss. To improve the sharpness of the synthesized face images, we also introduce a conditional adversarial loss. The discriminator tries to distinguish the fake image pair $\{\hat{I}^b, B^b\}$ from the real image pair $\{I^b, B^b\}$, and the generator tries to fool the discriminator:

$$\mathcal{L}_{\text{adv}} = \mathbb{E}_{I^b \sim P(I^b)} [\log D(I^b, B^b)] + \mathbb{E}_{\hat{I}^b \sim P(\hat{I}^b)} [\log(1 - D(\hat{I}^b, B^b))]. \quad (5)$$

In order to improve the ability of the discriminator, we adopt the multi-scale discriminant strategy [33]. It utilizes three discriminators to discriminate the synthesized images at three different scales.

Identity Preserving Loss. In order to further preserve the identity information of the synthesized faces, we adopt an identity preserving loss as [14]. Specifically, a pre-trained Light CNN [35] is introduced as a feature extractor D_{ip} . It forces the identity features of the synthesized face \hat{I}^b to be as close to the identity features of the real face I^b as possible. The identity preserving loss is formulated as:

$$\mathcal{L}_{\text{ip}} = \|D_{ip}^p(\hat{I}^b) - D_{ip}^p(I^b)\|_2^2 + \|D_{ip}^{fc}(\hat{I}^b) - D_{ip}^{fc}(I^b)\|_2^2. \quad (6)$$

where D_{ip}^p and D_{ip}^{fc} denote the output of last pooling layer and the fully connected layer, respectively.



Figure 4: Synthesis results (512×512) with different poses and expressions on the MVF-HQ database. For each image pair, the left is the original input and the right is the synthesized result. Zoom in for details.

3.3. Overall Loss

The boundary prediction stage and the disentangled face synthesis stage are trained separately. We first train the boundary prediction stage, and then utilize the predicted boundary to train the face synthesis stage. For the boundary prediction stage, the overall loss is:

$$\mathcal{L}_{bp} = \lambda_1 \mathcal{L}_{pix-bound} + \lambda_2 \mathcal{L}_{reg}. \quad (7)$$

For the the face synthesis stage, the overall loss is:

$$\mathcal{L}_{fs} = \alpha_1 \mathcal{L}_{thr} + \alpha_2 \mathcal{L}_{pix-mul} + \alpha_3 \mathcal{L}_{adv} + \alpha_4 \mathcal{L}_{ip}, \quad (8)$$

where λ_1 , λ_2 , α_1 , α_2 , α_3 and α_4 are the trade-off parameters.

4. Experiments

We evaluate our method on four databases. The details of databases and experimental settings are first introduced in Section 4.1. Then, qualitative and quantitative results are presented in Sections 4.2 and 4.3, respectively. Finally, experimental analysis is described in Section 4.4.

4.1. Databases and Settings

Classic Databases. Three classic face databases, including MultiPIE [10], RaFD [22] and CelebA-HQ [19], are chosen in our experiments. MultiPIE contains 337 identities under 15 poses, 20 illumination levels and 6 expressions. In our quantitative experiments, the division of training and testing sets are the same with the Setting 2 in [38], which only contains the natural expression. While in our qualitative experiments, we also use the data of the other 5 expressions. RaFD consists of 8,040 images, including 73 participants with 8 expressions, 3 gaze directions and 5 poses. We randomly select 10 identities as the testing set and use

Table 1: Comparisons of existing high-resolution face databases. Resolution means the maximum resolution of facial area that can be aligned.

Database	Images	Resolution	Identities	Poses	Expressions	Paired	Year
RaFD [22]	8,040	512×512	73	5	8	✓	2008
CelebA-HQ [19]	30,000	1024×1024	No Label	No Label	No Label	×	2017
FFHQ [20]	70,000	1024×1024	No Label	No Label	No Label	×	2018
MVF-HQ(Ours)	120,283	2048×2048	479	13	3	✓	2019

the remaining identities as the training set. CelebA-HQ is an in-the-wild database that consists of 30,000 celebrity images. Considering that most of the images in CelebA-HQ are frontal view, we utilize a 3D model [43] to make corresponding paired profiles. We randomly choose 3,000 images as the testing set and use the remaining images as the training set. Note that, all face images in MultiPIE are aligned to 128×128 resolution, while the images in RaFD and CelebA-HQ are aligned to 512×512 resolution.

MVF-HQ Database. In order to verify the effectiveness of our high fidelity method in the extreme case, we need a higher-resolution database with various poses and expressions. However, most of the existing face manipulation databases, e.g., MultiPIE, are limited in low-resolution. Although RaFD database can be aligned to 512×512 , the number (8,040 images) and the diversity (5 poses) are limited. The recently released high-resolution databases CelebA-HQ [19] and FFHQ [20] have greatly pushed forward the advances of high-resolution image synthesis, but the pose of these databases are also limited.

Therefore, we create a new high quality Multi-View Face (MVF-HQ) database that consists of 120,283 images¹ from 479 identities, including 13 poses, 3 expressions and 7 illuminations. The facial area of MVF-HQ can be aligned up to 2048×2048 resolution. The comparisons of existing public high-resolution face databases are presented

¹Some face images are removed while manually cleaning the database.



Figure 5: Synthesis results (1024×1024) on the MVF-HQ database. The lower right corner is the input face.

in Table 1, which shows the advantages of our MVF-HQ database. More information about this database is presented in supplementary materials. In our experiments, we randomly select 336 identities as the training set and the remaining 143 identities are treated as the testing set. There are no identity overlaps between training and testing. In addition, due to the limited GPU memory, we only conduct experiments at 512×512 and 1024×1024 resolutions. Higher resolution will be explored in our future work. We will release this database soon, along with 5 precise facial landmarks annotated by human.

Experimental Settings. The facial boundary image is obtained according to the facial landmarks. Thanks to the advances in facial landmark detection [5], we first detect 68 facial landmarks, and then connect the adjacent landmarks to obtain a boundary image. Meanwhile, pose vectors are calculated according to the detected facial landmarks. Moreover, we utilize the Action Units (AUs) [8] as our expression vectors, which are collected by the open source toolkit [1]. The pose estimator F_p and expression estimator F_e in Section 3.1 are pre-trained on the above four databases and a large-scale in-the-wild database CelebA [24]. Our method is implemented by Pytorch. The parameters λ_1 , λ_2 , α_1 , α_2 , α_3 and α_4 in Section 3.3 are set to 1, 0.1, 0.01, 50, 0.5 and 0.02, respectively. The parameter m in Eq. 3 is set to 7. The learning rate is set to 0.0002. Note that the high-resolution experiments on the MVF-HQ database are conducted on 8 NVIDIA Titan X GPUs with 12GB memory. Training takes about 12 days for 1024×1024 resolution and about 7 days for 512×512 resolution.

4.2. Qualitative Experiments

Experimental Results on the MultiPIE. According to the given conditional vectors, our method can render an input face to arbitrary pose and expression. Another state-of-the-art work to realize the similar task is CAPG-GAN

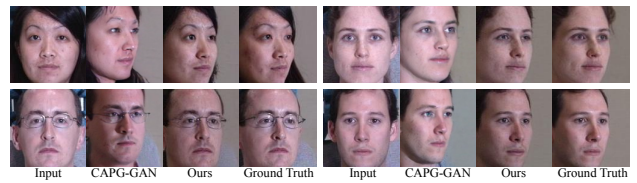


Figure 6: Visual comparisons with CAPG-GAN [14] on the MultiPIE Setting 2. Our method achieves better results in texture, e.g., the freckles in the first set of images. Zoom in for details.

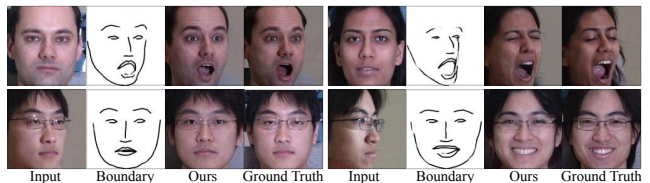


Figure 7: Synthesis results on the MultiPIE database. The boundary images are generated by our boundary prediction stage.

[14], which rotates a face to arbitrary pose controlled by 5 facial landmarks. CAPG-GAN directly concatenates the original faces and the target landmarks as input, and then feeds them into the generator. The comparison results between our method and CAPG-GAN are shown in Fig. 6. We can see that the synthesized images of CAPG-GAN can not preserve the texture well, e.g., the freckles in the first set of images. It is because that CAPG-GAN does not disentangle structure and texture in the latent space. On the contrary, the synthesized images by our method are closer to the ground truth. Besides, different from CAPG-GAN, our method can also render expression. Fig. 7 presents more synthesized results. We can observe that structure and texture of our synthesized images are all preserved well, even under extreme

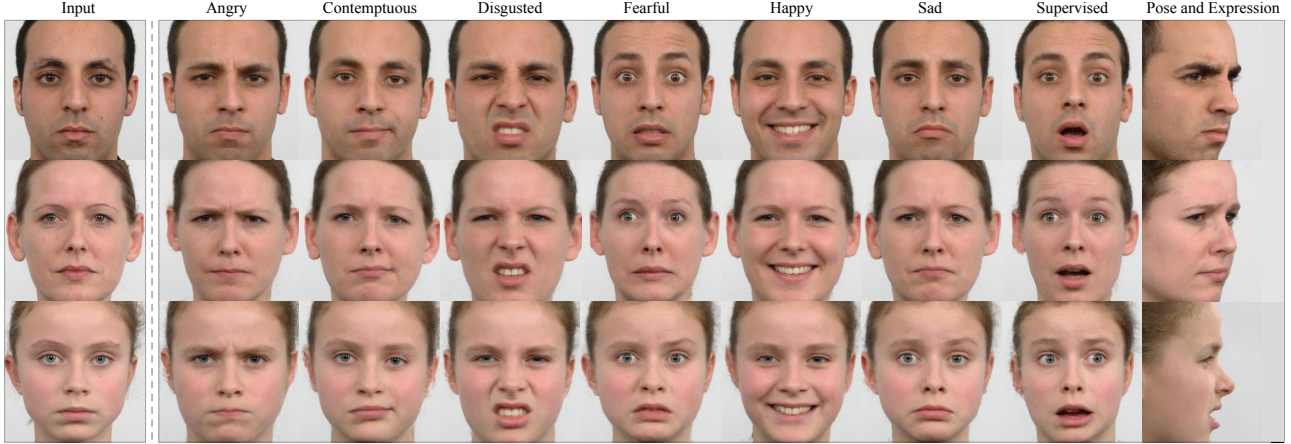


Figure 8: Facial expression and pose synthesis (512×512) on the RaFD database. The first column is the input, and the remaining columns are synthesized results with different expressions and poses.



Figure 9: Visual comparisons (512×512) with pix2pixHD [33] on the RaFD database (on the left) and MVF-QH database (on the right). Zoom in for details.

pose and expression.

Experimental Results on the RaFD. We first compare our method with pix2pixHD [33], which is a state-of-the-art high-resolution conditional image-to-image method, as shown in Fig. 9. Compared with pix2pixHD that lacks the guidance of structure, the synthesized images of our method have better quality. More results under different expressions and poses are shown in Fig. 8. Note that the number of training images in the RaFD database is small, which brings huge challenges to the network training. Fig. 8 and Fig. 9 show the ability of our method to achieve extreme high-resolution results in the case of limited training images.

Experimental Results on the MVF-HQ. The comparisons between our method and the pix2pixHD [33] are shown in Fig. 9. Compared with pix2pixHD, our method still maintains the degree of sharpness under such an extreme pose. More synthesis results of our method with different poses and expressions are shown in Fig. 1 and Fig. 4. We observe that our method can faithfully synthesize photo-realistic details, including the eyebrows, eyes, teeth, hair, etc. Moreover, we also extend our method to 1024×1024 resolution. As seen in Fig. 5, our method achieves great results in such a challenging situation.

Experimental Results on the CelebA-HQ. In order to further explore the expansibility of our method under in-the-wild situation, we perform visual comparison of face synthesis on the CelebA-HQ database. Fig. 10 shows the re-

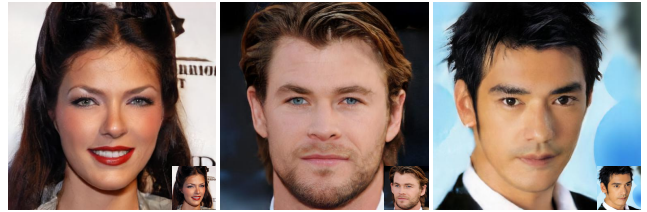


Figure 10: Synthesis results (512×512) on the CelebA-HQ database. The lower right corner is the input face.

sults of the synthesized frontal faces from the profiles. Our method can not only preserve the overall facial structures, but also recover the unseen textures.

4.3. Quantitative Experiments

In this section, we evaluate the identity preserving property and synthesis quality of our method. As shown in Fig. 7, our method can effectively restore the structure and texture from the profile faces, which can be used to improve face recognition under large poses [14, 36, 12]. Hence, we compare the face recognition accuracy of our method with the state-of-the-art face normalization methods, including 3D-PIM [42], CAPG-GAN [14], PIM [41], TP-GAN [16], FF-GAN [39] and DR-GAN [31] on the MultiPIE Setting 2. The comparison results are shown in Table 2. We can see that our method significantly outperforms its competitors, especially under extreme poses (75° and 90°). In addition, Table 3 further tabulates the results of different methods on the MVF-HQ database. Compared with the Setting 2 of MultiPIE that only contains natural expression, our new database is more challenging, because of the complicated expressions. We observe that our method still outperforms other state-of-the-art methods, including pix2pixHD [33] and CAPG-GAN. The face recognition results on the Mul-

Table 2: Comparisons of Rank-1 recognition rates (%) across views under the MultiPIE Setting2.

Method	$\pm 15^\circ$	$\pm 30^\circ$	$\pm 45^\circ$	$\pm 60^\circ$	$\pm 75^\circ$	$\pm 90^\circ$
DR-GAN [31]	94.0	90.1	86.2	83.2	-	-
FF-GAN [39]	94.6	92.5	89.7	85.2	77.2	61.2
TP-GAN [16]	98.7	98.1	95.4	87.7	77.4	64.6
PIM [41]	99.3	99.0	98.5	98.1	95.0	86.5
CAPG-GAN [14]	99.8	99.6	97.3	90.6	83.1	66.1
3D-PIM [42]	99.6	99.5	98.8	98.4	95.2	86.7
Ours	99.9	99.9	99.4	98.7	96.3	87.4

Table 3: Comparisons of Rank-1 recognition rates (%) across views under the MVF-HQ database.

Method	$\pm 15^\circ$	$\pm 30^\circ$	$\pm 45^\circ$	$\pm 60^\circ$	$\pm 75^\circ$	$\pm 90^\circ$
CAPG-GAN [14]	99.9	99.9	99.4	95.2	82.1	53.7
pix2pixHD [33]	98.5	97.5	93.3	86.1	67.4	39.0
Light CNN [35]	100	100	99.6	95.7	65.2	23.9
Ours	100	100	99.6	96.5	84.6	60.4

Table 4: The FID comparisons (lower is better) with CAPG-GAN [14], pix2pixHD [33] and our variants on the MVF-HQ database.

(a) Comparisons with the state-of-the-art methods.

	CAPG-GAN	pix2pixHD	Ours
FID	36.68	45.62	12.94

(b) Comparisons with our variants.

	w/o \mathcal{L}_{reg}	w/o \mathcal{L}_{thr}	w/o $\mathcal{L}_{pix-mul}$	w/o \mathcal{L}_{adv}	w/o \mathcal{L}_{ip}
FID	35.26	36.71	34.34	53.92	21.34

tiPIE and MVF-HQ suggest that our method can effectively improve the recognition performance under large poses.

Besides, in order to evaluate the quality of the synthesized images, we also compare Fréchet Inception Distance (FID) [13] with CAPG-GAN and pix2pixHD. We calculate the FID between the real faces and the synthesized faces. The results in Table 4 (a) further show that the high quality synthesis character of our method.

4.4. Experimental Analysis

Ablation Study. In this subsection, we study the roles of the five loss functions in our method. Both qualitative visualization results and quantitative FID results are reported for a comprehensive comparison. Fig. 11 shows the visual comparisons between our method and its five variants. We can see that without \mathcal{L}_{reg} , the generated boundary image, which does not belong to the database, will be unclear, resulting in an incomplete synthesized face. Without \mathcal{L}_{thr} , the local structures (e.g., the eyes and nose) are ambiguous and the textures are confused, indicating the usage of disentanglement. Without $\mathcal{L}_{pix-mul}$ and \mathcal{L}_{adv} , the synthesized faces display different degrees of blur, revealing the validity of

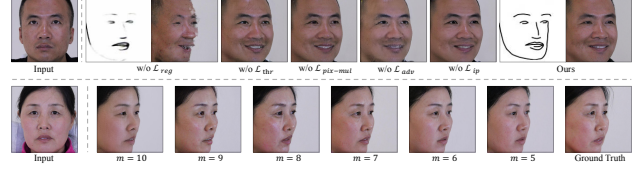


Figure 11: The results (512×512) of experimental analysis. The first row shows the results of ablation study and the second row presents the parameter analysis of m in Eq. 3.

multi-scale pixel-wise loss and multi-scale adversarial loss (Note that w/o $\mathcal{L}_{pix-mul}$ means only utilizing one scale pixel-wise loss.). Without \mathcal{L}_{ip} , the local textures (e.g., the beard) are few. Table 4 (b) further tabulates the FID results of different variants of our method. We can see that the FID will increase if one loss is not adopted, which is consistent with the visualization results. These visualization results and FID results verify that each component in our method is essential for extreme high-resolution face manipulation.

Parameter Analysis. As mentioned in Section 3.2, the parameter m of Eq. 3 affects the degree of disentanglement. We present the visual results when taking different values of m in Fig. 11. We can observe that when m is too large, the synthesized faces are blurred due to the weak disentanglement. On the contrary, when m is too small, the texture of the synthesized faces will be somewhat lost because of the too compact face features. The best result is obtained when $m = 7$.

5. Conclusion

This paper has developed a stage-wise framework for high fidelity face manipulation with extreme pose and expression. It simplifies the face manipulation into two correlated stages: a boundary prediction stage and a disentangled face synthesis stage. The first stage predicts the boundary image of the target face in a semi-supervised way, modeling pose and expression jointly. The second stage utilizes the predicted boundary to perform refined face synthesis. It introduces a proxy network and a novel feature threshold loss to disentangle the structure and texture in the latent space. Further, a new high-resolution MVF-HQ database is created to promote the development of high-resolution face synthesis. Extensive experiments show that our method pushes forward the advance of extreme face manipulation from 128×128 resolution to 1024×1024 resolution, and significantly improves the face recognition performance under large poses.

References

- [1] T. Baltrusaitis, A. Zadeh, Y. C. Lim, and L.-P. Morency. Openface 2.0: Facial behavior analysis toolkit. In *FG*, 2018.
- [2] J. Bao, D. Chen, F. Wen, H. Li, and G. Hua. Towards open-set identity preserving face synthesis. In *CVPR*, 2018.

- [3] V. Blanz, C. Basso, T. Poggio, and T. Vetter. Reanimating faces in images and video. In *CGF*, 2003.
- [4] A. Brock, J. Donahue, and K. Simonyan. Large scale gan training for high fidelity natural image synthesis. In *ICLR*, 2019.
- [5] A. Bulat and G. Tzimiropoulos. How far are we from solving the 2d & 3d face alignment problem? (and a dataset of 230,000 3d facial landmarks). In *ICCV*, 2017.
- [6] C. Cao, Y. Weng, S. Zhou, Y. Tong, and K. Zhou. Faceware-house: A 3d facial expression database for visual computing. *TVCG*, 2014.
- [7] Y. Choi, M. Choi, M. Kim, J.-W. Ha, S. Kim, and J. Choo. Stargan: Unified generative adversarial networks for multi-domain image-to-image translation. In *CVPR*, 2018.
- [8] E. Friesen and P. Ekman. Facial action coding system: a technique for the measurement of facial movement. *Palo Alto*, 1978.
- [9] I. Goodfellow, J. Pouget-Abadie, M. Mirza, B. Xu, D. Warde-Farley, S. Ozair, A. Courville, and Y. Bengio. Generative adversarial nets. In *NIPS*, 2014.
- [10] R. Gross, I. Matthews, J. Cohn, T. Kanade, and S. Baker. Multi-pie. *Image and Vision Computing*, 2010.
- [11] K. He, X. Zhang, S. Ren, and J. Sun. Deep residual learning for image recognition. In *CVPR*, 2016.
- [12] R. He, X. Wu, Z. Sun, and T. Tan. Wasserstein cnn: Learning invariant features for nir-vis face recognition. *TPAMI*, 2018.
- [13] M. Heusel, H. Ramsauer, T. Unterthiner, B. Nessler, G. Klambauer, and S. Hochreiter. Gans trained by a two time-scale update rule converge to a nash equilibrium. In *NIPS*, 2017.
- [14] Y. Hu, X. Wu, B. Yu, R. He, and Z. Sun. Pose-guided photo-realistic face rotation. In *CVPR*, 2018.
- [15] H. Huang, Z. Li, R. He, Z. Sun, and T. Tan. Introvae: Introspective variational autoencoders for photographic image synthesis. In *NIPS*, 2018.
- [16] R. Huang, S. Zhang, T. Li, and R. He. Beyond face rotation: Global and local perception gan for photorealistic and identity preserving frontal view synthesis. In *ICCV*, 2017.
- [17] P. Isola, J.-Y. Zhu, T. Zhou, and A. A. Efros. Image-to-image translation with conditional adversarial networks. In *CVPR*, 2017.
- [18] Y. Jo and J. Park. Sc-fegan: Face editing generative adversarial network with user’s sketch and color. *arXiv:1902.06838*, 2019.
- [19] T. Karras, T. Aila, S. Laine, and J. Lehtinen. Progressive growing of gans for improved quality, stability, and variation. In *ICLR*, 2018.
- [20] T. Karras, S. Laine, and T. Aila. A style-based generator architecture for generative adversarial networks. *arXiv:1812.04948*, 2018.
- [21] I. Kemelmacher-Shlizerman, S. Suwajanakorn, and S. M. Seitz. Illumination-aware age progression. In *CVPR*, 2014.
- [22] O. Langner, R. Dotsch, G. Bijlstra, D. H. Wigboldus, S. T. Hawk, and A. Van Knippenberg. Presentation and validation of the radboud faces database. *Cognition and Emotion*, 2010.
- [23] P. Li, Y. Hu, R. He, and Z. Sun. Global and local consistent wavelet-domain age synthesis. *TIFS*, 2018.
- [24] Z. Liu, P. Luo, X. Wang, and X. Tang. Deep learning face attributes in the wild. In *ICCV*, 2015.
- [25] A. Pumarola, A. Agudo, A. M. Martinez, A. Sanfeliu, and F. Moreno-Noguer. Animation: Anatomically-aware facial animation from a single image. In *ECCV*, 2018.
- [26] I. Radosavovic, P. Dollár, R. Girshick, G. Gkioxari, and K. He. Data distillation: Towards omni-supervised learning. In *CVPR*, 2018.
- [27] Y. Shen, P. Luo, J. Yan, X. Wang, and X. Tang. Faceid-gan: Learning a symmetry three-player gan for identity-preserving face synthesis. In *CVPR*, 2018.
- [28] Z. Shu, M. Sahasrabudhe, R. Alp Guler, D. Samaras, N. Paragios, and I. Kokkinos. Deforming autoencoders: Unsupervised disentangling of shape and appearance. In *ECCV*, 2018.
- [29] L. Song, Z. Lu, R. He, Z. Sun, and T. Tan. Geometry guided adversarial facial expression synthesis. In *ACMM*, 2018.
- [30] J. Thies, M. Zollhofer, M. Stamminger, C. Theobalt, and M. Nießner. Face2face: Real-time face capture and reenactment of rgb videos. In *CVPR*, 2016.
- [31] L. Tran, X. Yin, and X. Liu. Disentangled representation learning gan for pose-invariant face recognition. In *CVPR*, 2017.
- [32] T.-C. Wang, M.-Y. Liu, J.-Y. Zhu, G. Liu, A. Tao, J. Kautz, and B. Catanzaro. Video-to-video synthesis. In *NIPS*, 2018.
- [33] T.-C. Wang, M.-Y. Liu, J.-Y. Zhu, A. Tao, J. Kautz, and B. Catanzaro. High-resolution image synthesis and semantic manipulation with conditional gans. In *CVPR*, 2018.
- [34] Y. Wang, L. Zhang, Z. Liu, G. Hua, Z. Wen, Z. Zhang, and D. Samaras. Face relighting from a single image under arbitrary unknown lighting conditions. *TPAMI*, 2009.
- [35] X. Wu, R. He, Z. Sun, and T. Tan. A light cnn for deep face representation with noisy labels. *TIFS*, 2018.
- [36] X. Wu, H. Huang, V. M. Patel, R. He, and Z. Sun. Disentangled variational representation for heterogeneous face recognition. In *AAAI*, 2019.
- [37] F. Yang, J. Wang, E. Shechtman, L. Bourdev, and D. Metaxas. Expression flow for 3d-aware face component transfer. *TOG*, 2011.
- [38] J. Yim, H. Jung, B. Yoo, C. Choi, D. Park, and J. Kim. Rotating your face using multi-task deep neural network. In *CVPR*, 2015.
- [39] X. Yin, X. Yu, K. Sohn, X. Liu, and M. Chandraker. Towards large-pose face frontalization in the wild. In *ICCV*, 2017.
- [40] F. Zhang, T. Zhang, Q. Mao, and C. Xu. Joint pose and expression modeling for facial expression recognition. In *CVPR*, 2018.
- [41] J. Zhao, Y. Cheng, Y. Xu, L. Xiong, J. Li, F. Zhao, K. Jayashree, S. Pranata, S. Shen, J. Xing, S. Yan, and J. Feng. Towards pose invariant face recognition in the wild. In *CVPR*, 2018.
- [42] J. Zhao, L. Xiong, Y. Cheng, Y. Cheng, J. Li, L. Zhou, Y. Xu, J. Karlekar, S. Pranata, S. Shen, J. Xing, S. Yan, and J. Feng. 3d-aided deep pose-invariant face recognition. In *IJCAI*, 2018.
- [43] X. Zhu, Z. Lei, X. Liu, H. Shi, and S. Z. Li. Face alignment across large poses: A 3d solution. In *CVPR*, 2016.

6. Supplementary Materials

6.1. Multi-View Face (MVF-HQ) Database

The data acquisition system is shown in Fig. 12 (a). It consists of 13 digital cameras (Canon EOS 1300D/1500D with 55mm prime lens), locating at the same height with head. The angle between two cameras is 15° . All the cameras are connected with the computers to take photos simultaneously. The original images with different views are shown in Fig. 12(c). The resolution is 6000×4000 and the facial area can reach 2048×2048 . Besides, 7 illuminations are also provided in the acquisition system, including above, front, front-above, front-below, behind, left and right. A total of 479 volunteers participated in the database collection and all the volunteers have signed a license. Each participant is asked to display three facial expressions, including neutral, smile and surprise, as shown in Fig. 12 (b). Therefore, the total number of images is 130,767 ($479 \text{ identities} \times 3 \text{ expressions} \times 13 \text{ views} \times 7 \text{ illuminations}$). After manually cleaning the database, the final number of images is 120,283. In addition, we also manually mark 5 facial landmarks for each image.

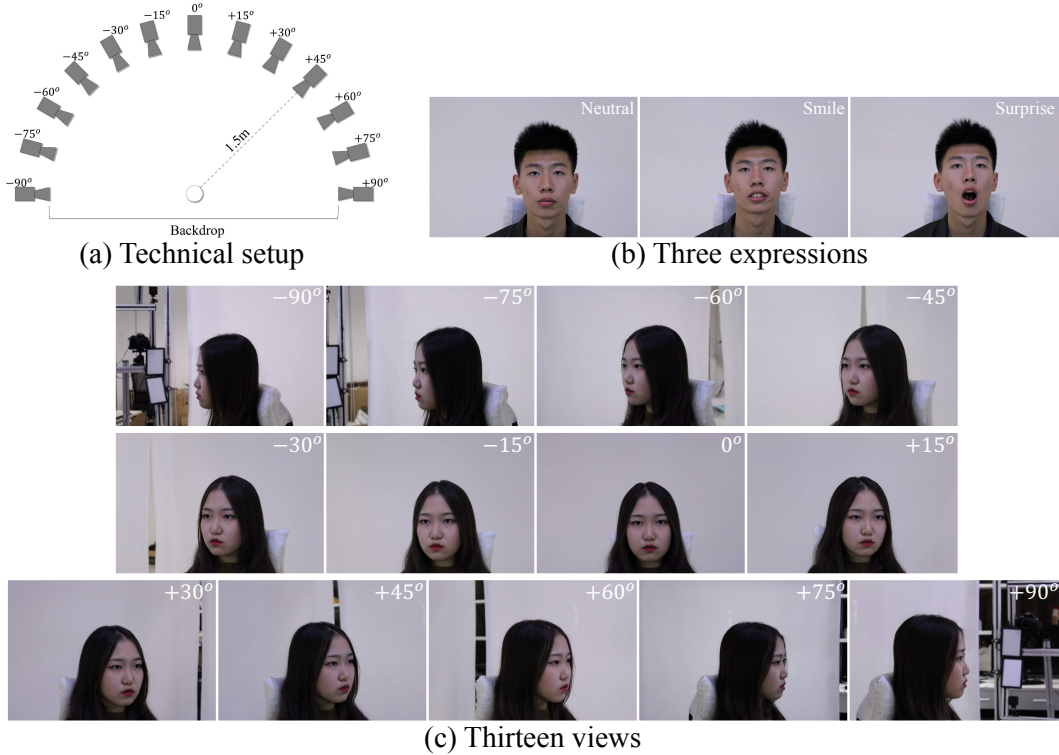


Figure 12: Technical setup and examples (6000×4000 resolution) of our MVF-HQ database. (a) Technical setup. (b) Examples for the three expressions. (c) Examples for the thirteen views.

6.2. Network Architectures

The network architectures of generators G_{enc}^I , G_{dec}^I and discriminator are presented in Table 5, Table 6 and Table 7, respectively. *Conv* contains convolution, instance normalization and ReLU, while *Conv** just contains convolution. Meanwhile, *Deconv* contains deconvolution with one output padding, instance normalization and ReLU. In addition, the architecture of G_{enc}^B is the same with G_{enc}^I , except the number of channels in the convolution layer is half of G_{enc}^I . *Res-block* denotes a residual block [11]. The output shape in Table 4 is for the input resolution of 1024×1024 , the same architecture is directly applied to the other two scales of the input image (512×512 and 256×256), same as [33].

6.3. Additional Results on the CelebA-HQ

Due to the effects of uncontrolled variants, such as illumination and background, high-resolution face frontalization under the in-the-wild setting is challenging. More visualization results (512×512 resolution) on the CelebA-HQ database are shown in Fig. 13 and Fig. 14, which demonstrate the effectiveness of our method in the uncontrolled situation.

Table 5: The architecture of G_{enc}^I .

G_{enc}^I	Filter/Stride/Padding	Output Shape
Input image	-	$3 \times 1024 \times 1024$
Conv	$7 \times 7 / 1 / 3$	$32 \times 1024 \times 1024$
Conv	$3 \times 3 / 2 / 1$	$64 \times 512 \times 512$
Conv	$3 \times 3 / 2 / 1$	$128 \times 256 \times 256$
Conv	$3 \times 3 / 2 / 1$	$256 \times 128 \times 128$
Conv	$3 \times 3 / 2 / 1$	$512 \times 64 \times 64$
Conv	$3 \times 3 / 2 / 1$	$256 \times 32 \times 32$
Conv	$3 \times 3 / 2 / 1$	$128 \times 16 \times 16$
Conv	$3 \times 3 / 2 / 1$	$128 \times 8 \times 8$

Table 6: The architecture of G_{dec}^I .

G_{dec}^I	Filter/Stride/Padding	Output Shape
Input feature	-	$192 \times 8 \times 8$
Res-block	$3 \times 3 / 1 / 1$	$512 \times 8 \times 8$
Res-block	$3 \times 3 / 1 / 1$	$512 \times 8 \times 8$
Res-block	$3 \times 3 / 1 / 1$	$512 \times 8 \times 8$
Deconv	$3 \times 3 / 2 / 1$	$512 \times 16 \times 16$
Deconv	$3 \times 3 / 2 / 1$	$512 \times 32 \times 32$
Deconv	$3 \times 3 / 2 / 1$	$256 \times 64 \times 64$
Deconv	$3 \times 3 / 2 / 1$	$256 \times 128 \times 128$
Deconv	$3 \times 3 / 2 / 1$	$128 \times 256 \times 256$
Deconv	$3 \times 3 / 2 / 1$	$64 \times 512 \times 512$
Deconv	$3 \times 3 / 2 / 1$	$32 \times 1024 \times 1024$
Conv*	$7 \times 7 / 1 / 3$	$3 \times 1024 \times 1024$

Table 7: The architecture of discriminator.

Discriminator	Filter/Stride/Padding	Output Shape
Input image	-	$6 \times 1024 \times 1024$
Conv	$4 \times 4 / 2 / 1$	$64 \times 512 \times 512$
Conv	$4 \times 4 / 2 / 1$	$128 \times 256 \times 256$
Conv	$4 \times 4 / 2 / 1$	$256 \times 128 \times 128$
Conv	$4 \times 4 / 1 / 1$	$512 \times 127 \times 127$
Conv*	$4 \times 4 / 1 / 1$	$1 \times 126 \times 126$

6.4. Additional Results on the MVF-HQ

More face rotation results on the MVF-HQ database are presented in Fig. 15 (512×512 resolution), Fig. 16 (1024×1024 resolution) and Fig. 17 (1024×1024 resolution). The results (512×512 resolution) of continuous pose change are shown as a GIF file in our folder (the frontal image is the original input face and the others are synthesized).

6.5. Additional Results on the MultiPIE

Fig. 18 shows the results of rotating an input frontal face to arbitrary poses and expressions. We can observe that the synthesis results are impressive, even under the extreme poses and expressions. Fig. 19 presents the results of frontalizing a profile face (90°) with expression changes. It is challenging to frontalize a profile face under 90° , let alone changing the expression at the same time. We can see that the results of our method are very close to the ground truth.

6.6. Additional Results on the RaFD

By continuously controlling the expression vector, our method can realize continuous expression change. The results (512×512 resolution) are shown as a GIF file in our folder (the first image with neutral expression is the original face and the others are synthesized).



Figure 13: Visualization results (512×512 resolution) on the CelebA-HQ database. The lower right corner is the input profile.

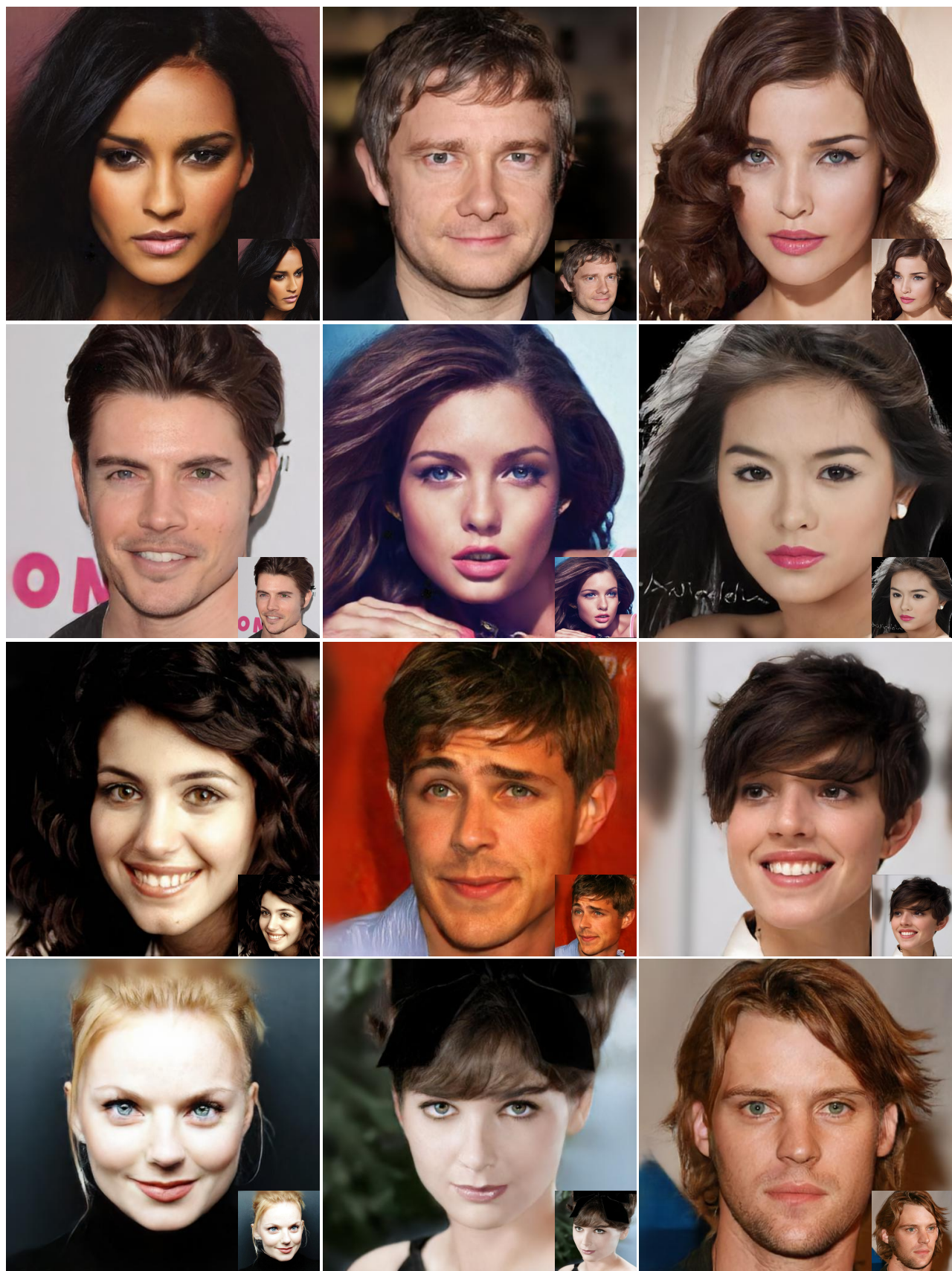


Figure 14: Visualization results (512×512 resolution) on the CelebA-HQ database. The lower right corner is the input profile.



Figure 15: Visualization results (512×512 resolution) on the MVF-HQ database. The lower right corner is the input face.

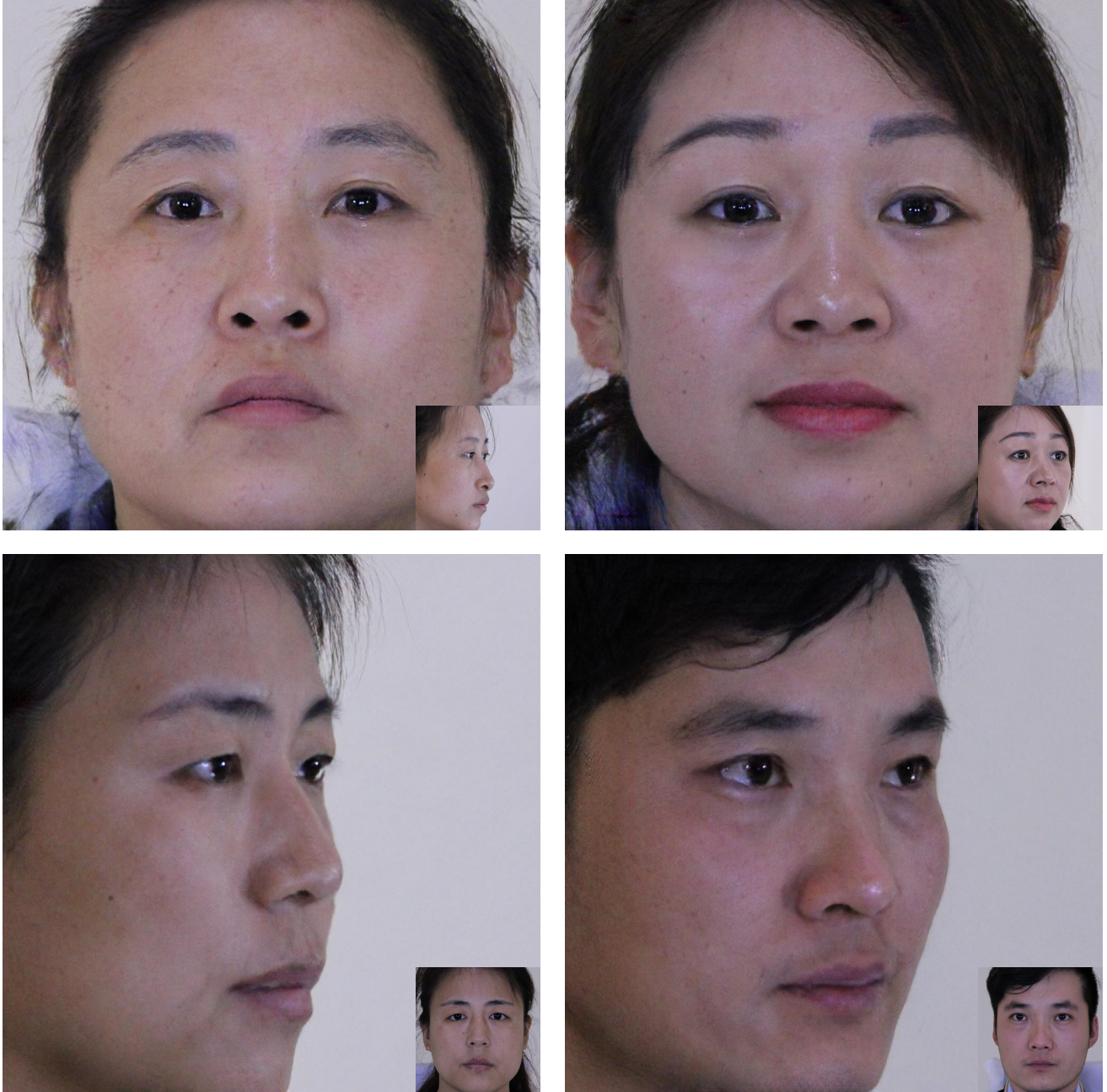


Figure 16: Visualization results (1024×1024 resolution) on the MVF-HQ database. The lower right corner is the input face.



Figure 17: Visualization results (1024×1024) on the MVF-HQ database. The lower right corner is the input face.

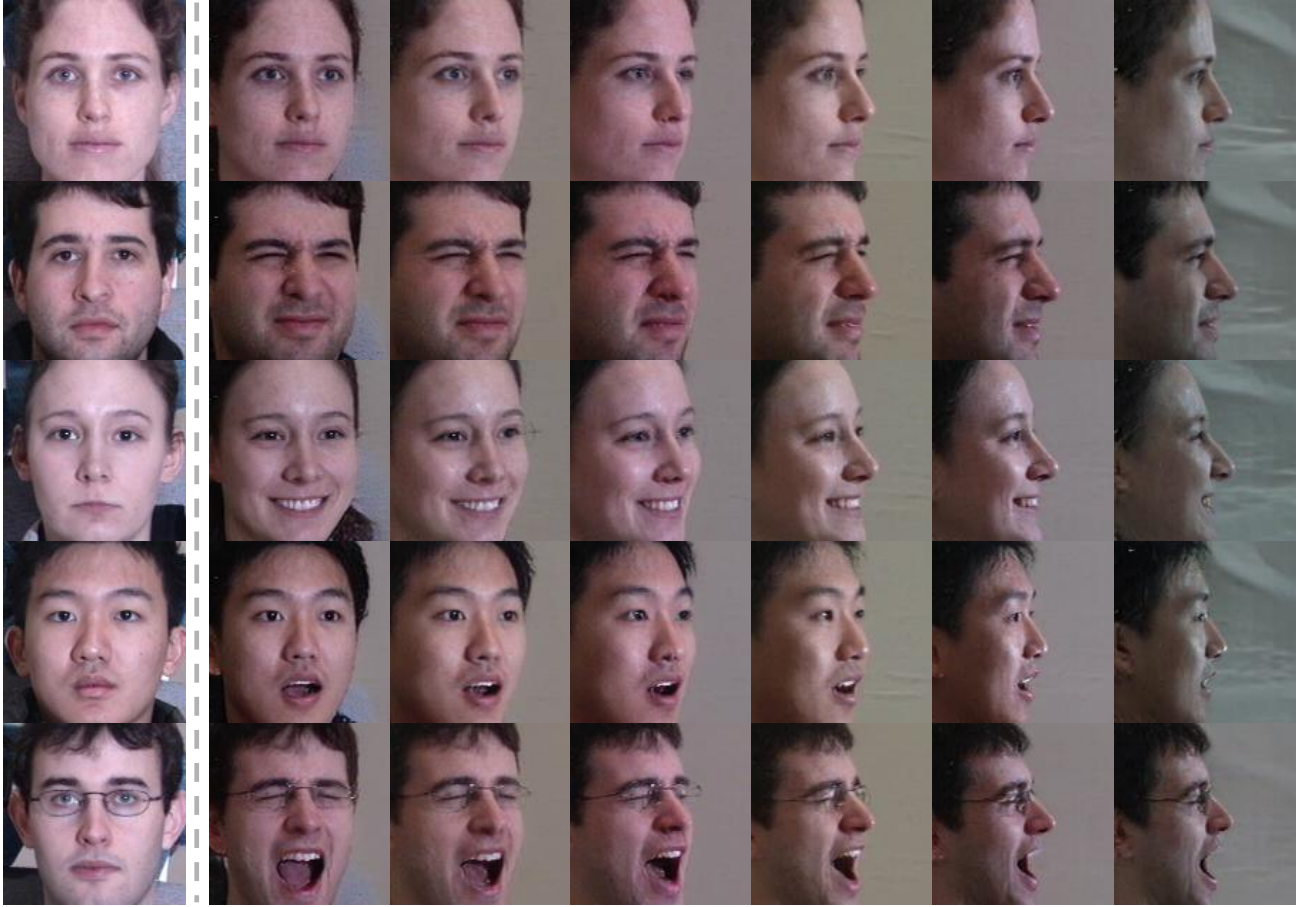


Figure 18: Visualization results on the MultiPIE database. The first column is the input, and the remaining columns are the synthesized results.



Figure 19: Visual results on the MultiPIE database. For each image set, the first image is the input, the second image is the synthesized result, and the last image is the ground truth.